Supplementary Material

Gradient engineering in proton exchange membrane fuel cell cathodes: an electrochemical study of charge transfer, mass transport, and Pt utilization

Adib Caidi[1], Thomas Lange[1,*], Ivan Radev[1,2], Kerstin Grimm[1], Fatih Özcan[3,4], Volker Peinecke[1], Doris Segets[3,4,*]

[1]The Hydrogen and Fuel Cell Center (ZBT GmbH), Duisburg 47057, Germany.
[2]Institute of Electrochemistry and Energy Systems "Academician Evgeni Budevski", Bulgarian Academy of Sciences, Sofia 1113, Bulgaria.
[3]Institute for Energy and Materials Processes - Particle Science and Technology (EMPI-PST), University of Duisburg-Essen, Duisburg 47057, Germany.
[4]Center for Nanointegration Duisburg-Essen (CENIDE), Duisburg 47057, Germany.

***Correspondence to:** Dr. Thomas Lange, The Hydrogen and Fuel Cell Center (ZBT GmbH), Carl-Benz-Strasse 201, Duisburg 47057, Germany. E-mail: t.lange@zbt.de; Prof./Dr. Doris Segets, Institute for Energy and Materials Processes - Particle Science and Technology (EMPI-PST), University of Duisburg-Essen, Carl-Benz-Strasse 199, Duisburg 47057, Germany; Center for Nanointegration Duisburg-Essen (CENIDE), Carl-Benz-Strasse 199, Duisburg 47057, Germany. E-mail: doris.segets@uni-due.de

SI 1: Micro X-ray Fluorescence Spectroscopy (µXRF) for Pt-Loading Analysis

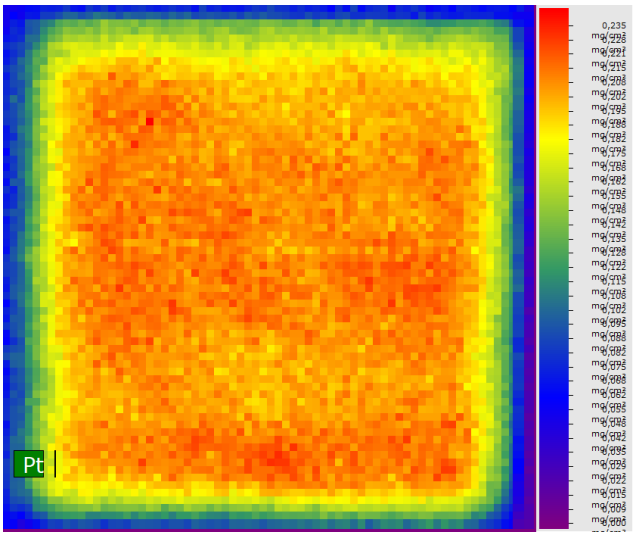

Figure S1 Example of Pt-lading distribution measured via µXRF.

The measurements were conducted using an X-ray source operated at 800 mA and 35 kV. The sample was scanned at a spatial resolution of 100 µm per pixel with a scan speed of 5 mm/s. To minimize measurement noise and interference, the sample was mounted in a suspended holder within the µXRF instrument.

Subsequently, the sample was measured under vacuum conditions using the aforementioned parameters. Data evaluation was initially performed using relative intensity values based on an internal reference database, without any mechanical motion during analysis.

Quantitative elemental mapping was then carried out using an internal standard that had been previously validated by an external laboratory. Elemental concentrations were determined either as an average over a defined area or for the entire sample surface.

SI 2: Fitting example for EIS Data

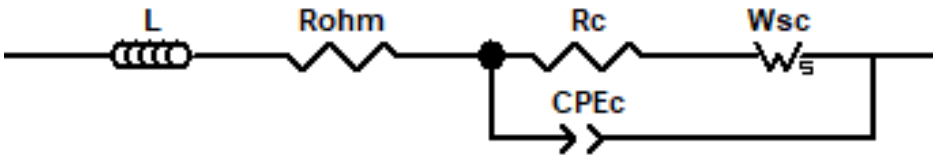

Figure S2 Equivalent circuit model for EIS analysis.

- L – the inductance of the wires and the cell, capturing the effects of magnetic fields generated by current flow within the PEMFC.
- R_{ohm} – the total ohmic resistance in the PEM-FC, including contributions from contact resistances, electronic resistances in the electrodes, and protonic resistances through the membrane.
- R_c – the charge transfer resistance at the cathode, indicative of the electrochemical reaction rate for the oxygen reduction reaction (ORR).
- CPEc – the constant phase element at the cathode, which accounts for the deviation from ideal capacitive behavior due to the porous structure of the cathode. It models non-uniform charge distribution.
- Wsc – the short Warburg element, representing the impedance associated with finite diffusion within the PEM-FC cathode. It describes the impedance response when diffusion layers are limited in thickness, often linked to mass transport in the CLs or diffusion media.

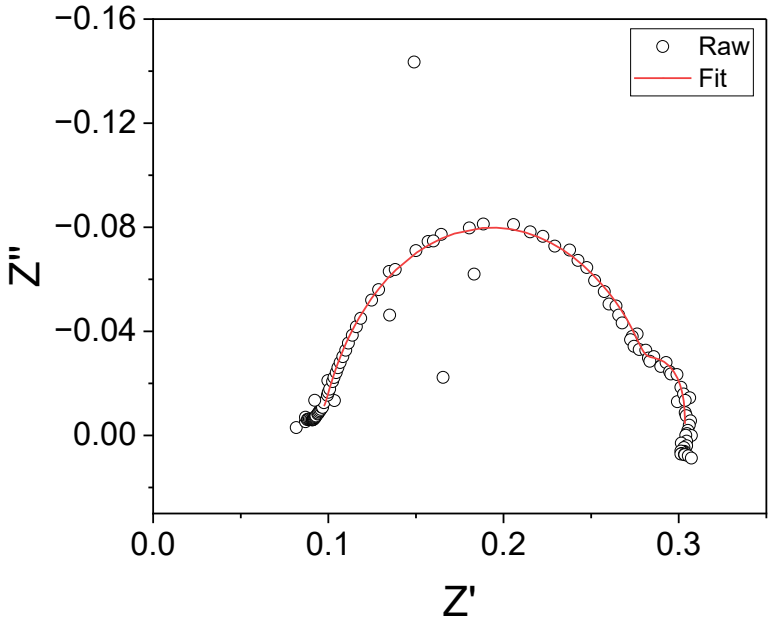

Figure S3 Example of fitting data for EIS-Spectroscopy.

SI 3: Polarization Curves at Pol 1 and Pol 2 of the investigated Samples

- **Pt/XC72R**

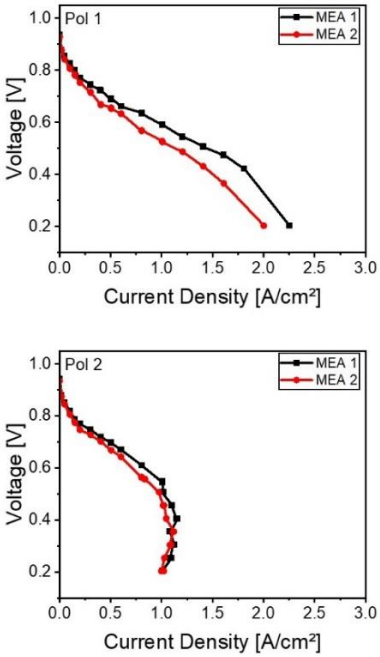

Figure S4 Polarization curves of EW 720 at I/C 0.7 at Pol 1 and Pol 2.

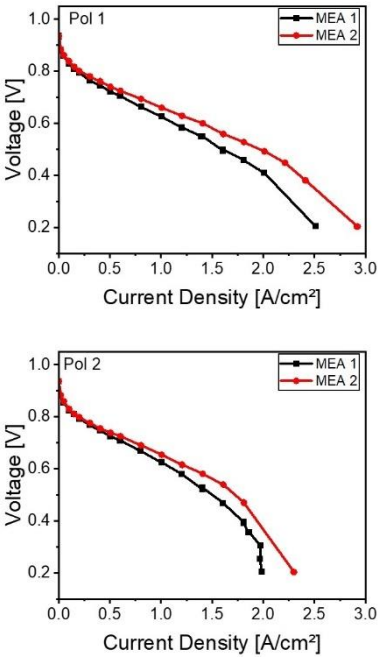

Figure S5 Polarization curves of EW 830 at I/C 0.7 at Pol 1 and Pol 2.

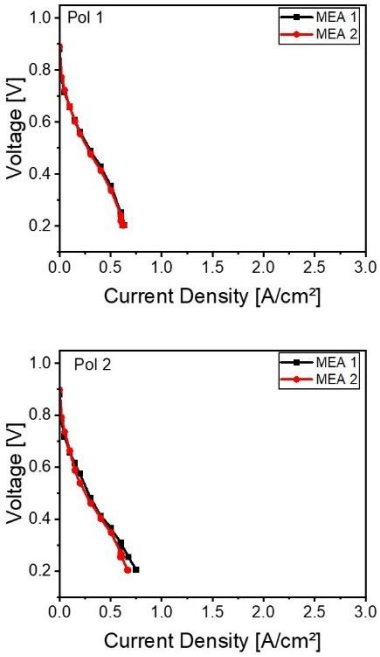

Figure S6 Polarization curves of EW 980 at I/C 0.7 at Pol 1 and Pol 2.

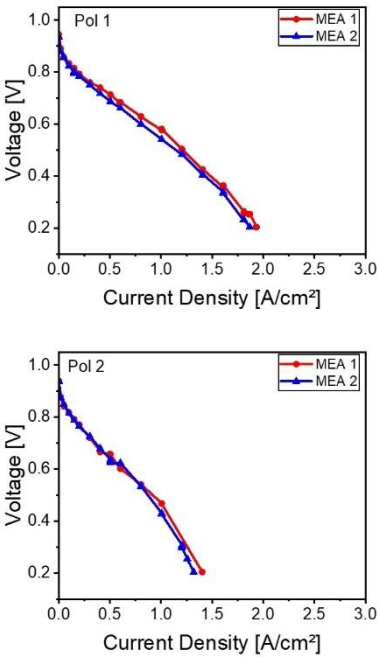

Figure S7 Polarization curves of EW 720 at I/C 0.9 at Pol 1 and Pol 2.

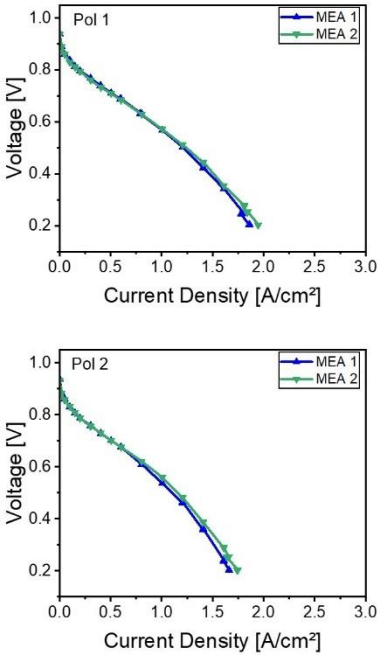

Figure S8 Polarization curves of EW 830 at I/C 0.9 at Pol 1 and Pol 2.

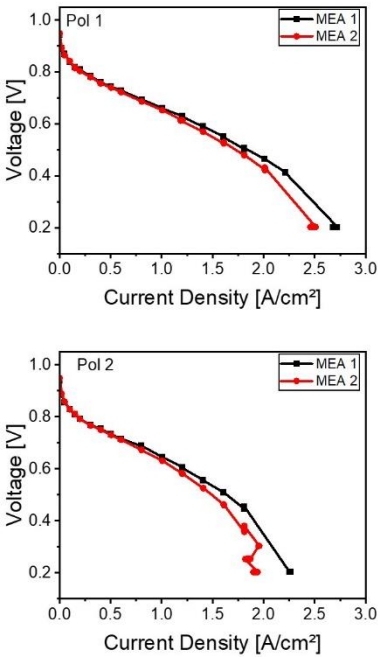

Figure S9 Polarization curves of EW 980 at I/C 0.9 at Pol 1 and Pol 2.

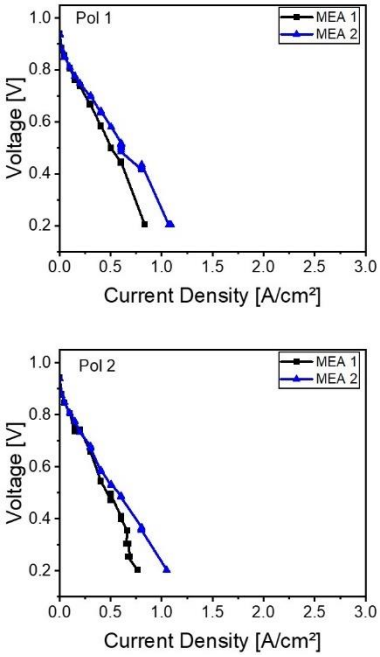

Figure S10 Polarization curves of EW 720 at I/C 1.1 at Pol 1 and Pol 2.

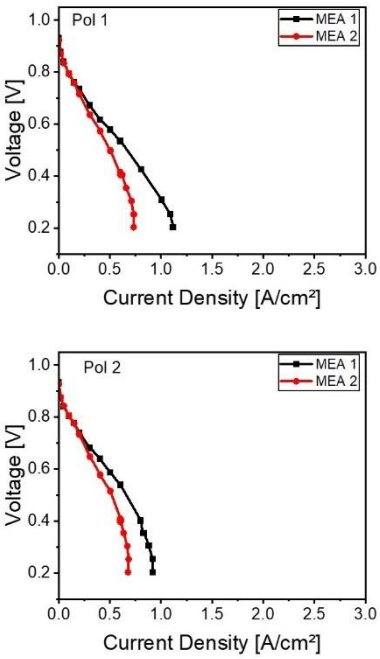

Figure S11 Polarization curves of EW 830 at I/C 1.1 at Pol 1 and Pol 2.

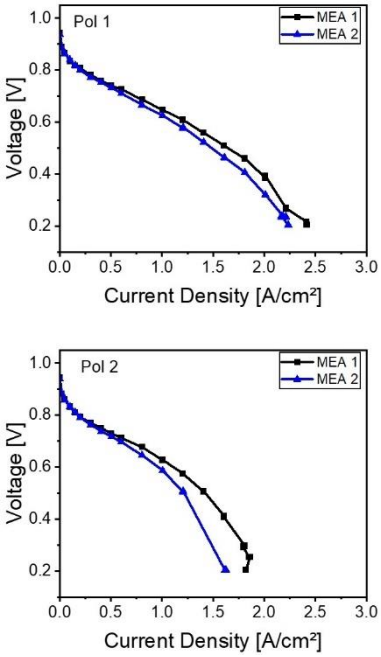

Figure S12 Polarization curves of EW 980 at I/C 1.1 at Pol 1 and Pol 2.

- **Pt/MSAC**

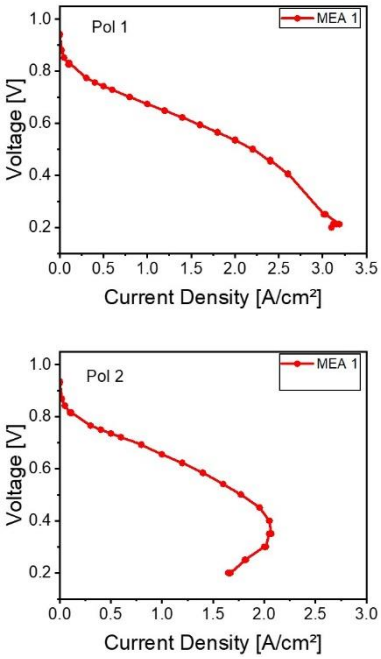

Figure S13 Polarization curves of EW 720 at I/C 0.7 at Pol 1 and Pol 2.

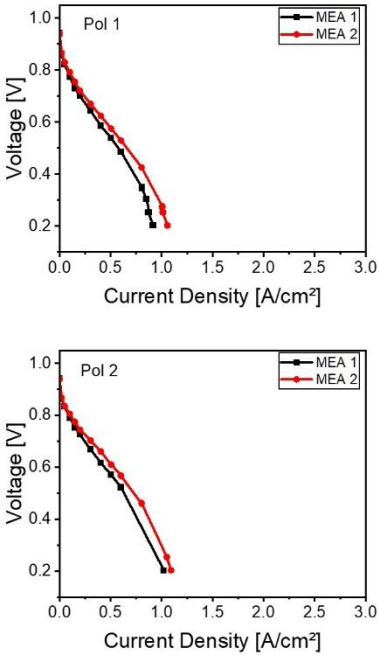

Figure S14 Polarization curves of EW 830 at I/C 0.7 at Pol 1 and Pol 2.

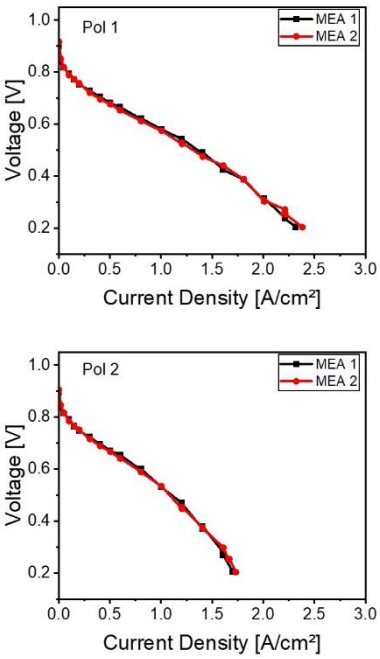

Figure S15 Polarization curves of EW 980 at I/C 0.7 at Pol 1 and Pol 2.

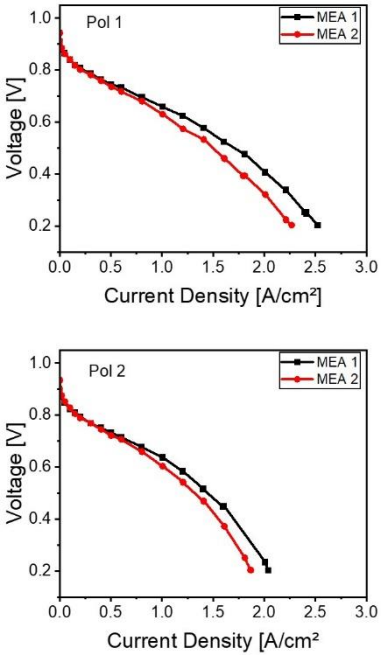

Figure S16 Polarization curves of EW 720 at I/C 0.9 at Pol 1 and Pol 2.

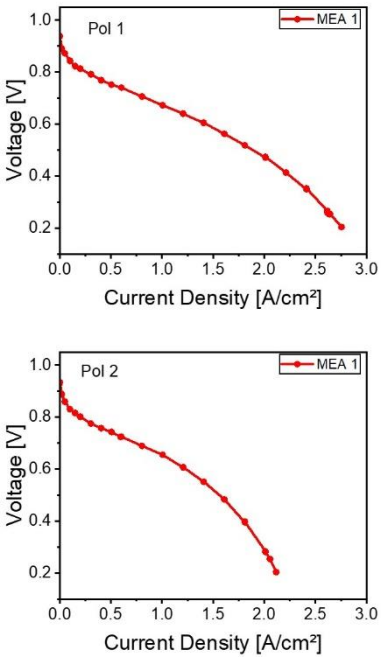

Figure S17 Polarization curves of EW 830 at I/C 0.9 at Pol 1 and Pol 2.

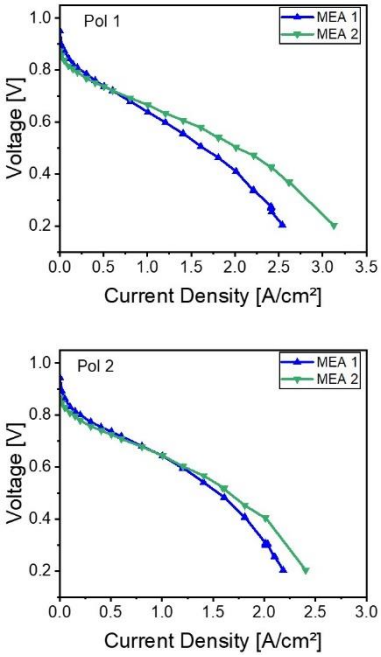

Figure S18 Polarization curves of EW 980 at I/C 0.9 at Pol 1 and Pol 2.

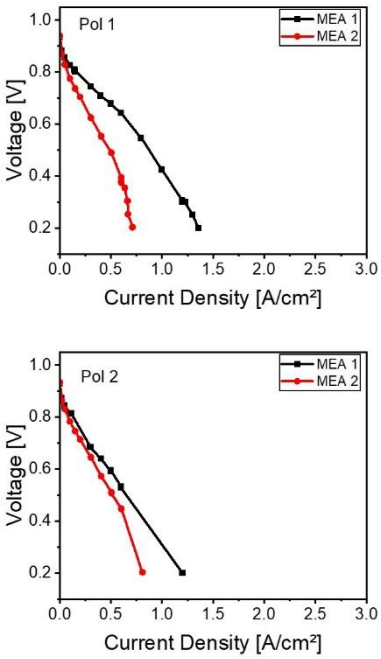

Figure S19 Polarization curves of EW 720 at I/C 1.1 at Pol 1 and Pol 2.

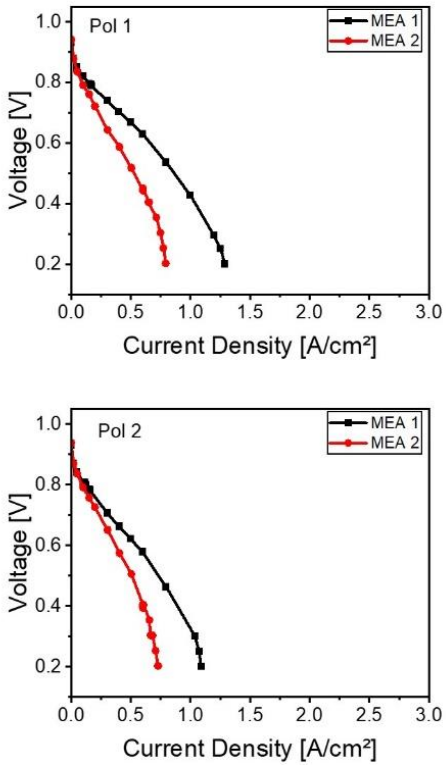

Figure S20 Polarization curves of EW 830 at I/C 1.1 at Pol 1 and Pol 2.

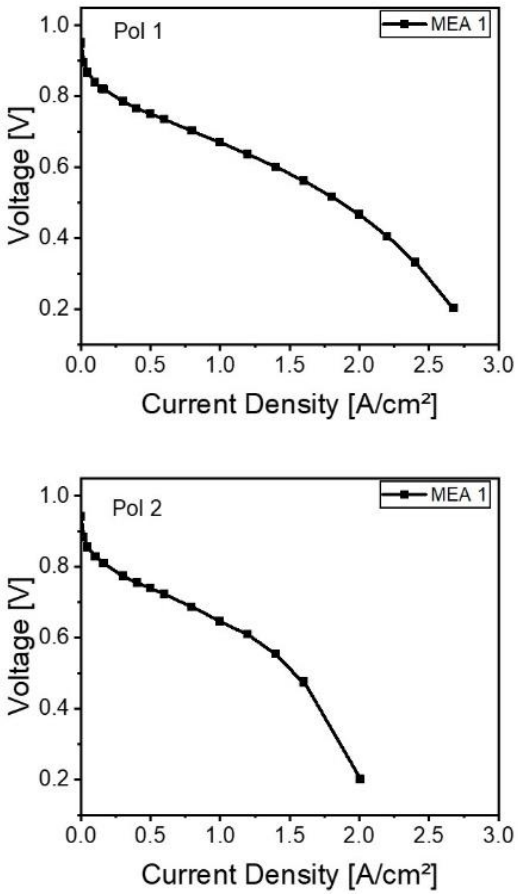

Figure S21 Polarization curves of EW 980 at I/C 1.1 at Pol 1 and Pol 2.

- **I/C Gradient**

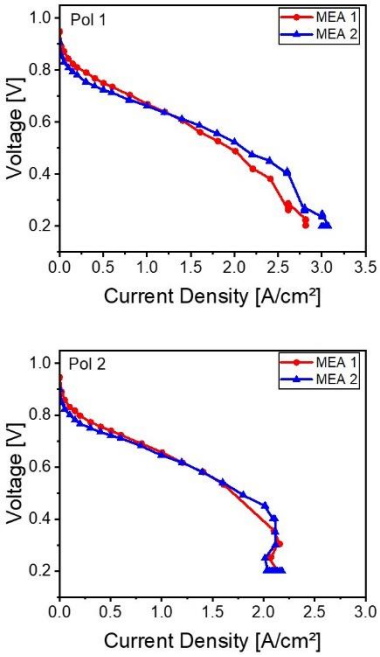

Figure S22 Polarization curves for the I/C gradient at Pol 1 and Pol 2.

- **EW Gradient**

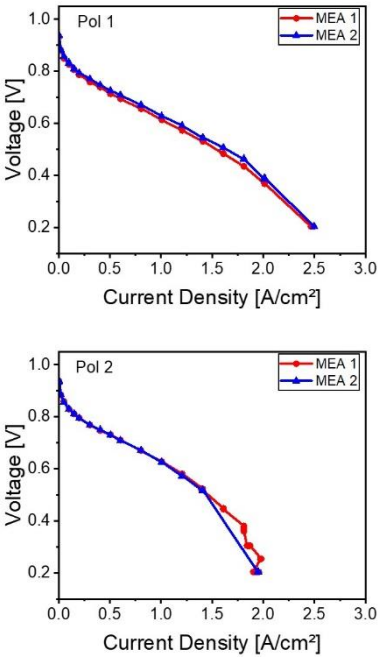

Figure S23 Polarization curves for the EW gradient at Pol 1 and Pol 2.

- **Simultaneous I/C & EW gradient**

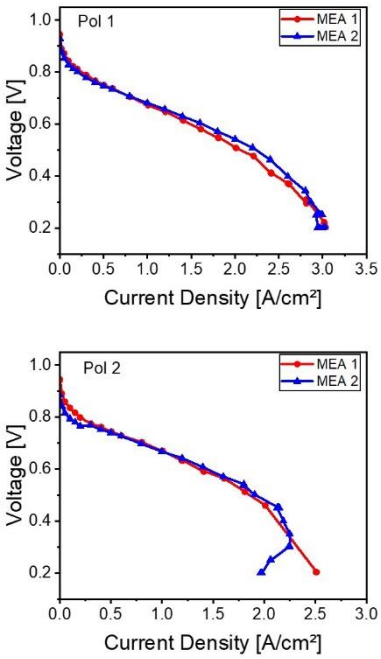

Figure S24 Polarization curves for the simultaneous I/C & EW gradient at Pol 1 and Pol 2.

- **Pt/C loading gradient**

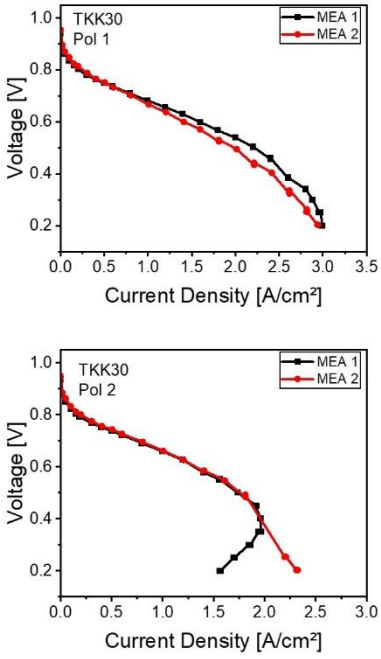

Figure S25 Polarization curves for TKK30 at Pol 1 and Pol 2.

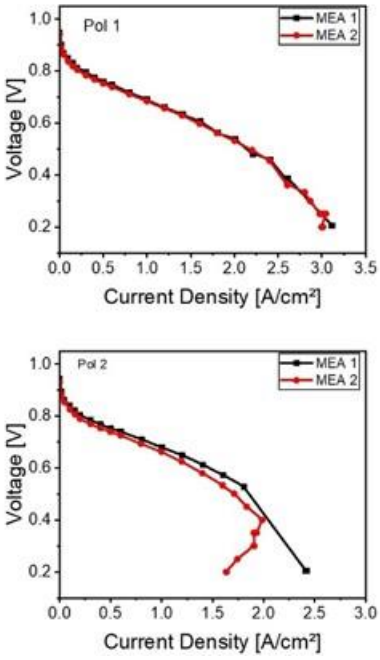

Figure S26 Polarization curves for TKK40 at Pol 1 and Pol 2.

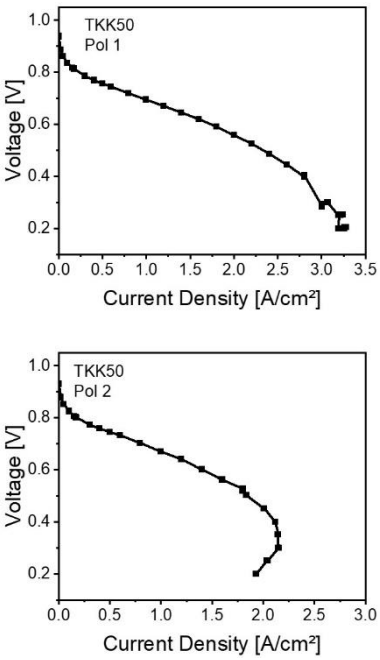

Figure S27 Polarization curves for TKK50 at Pol 1 and Pol 2.

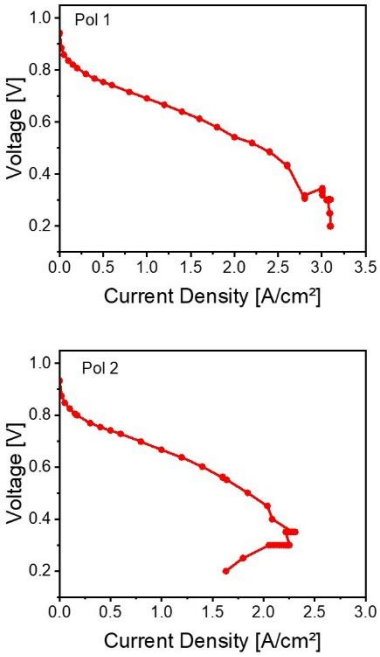

Figure S28 Polarization curves for Pt/C gradient at Pol 1 and Pol 2.

- **Simultaneous I/C & EW & Pt/C Gradients under Pol 2 conditions**

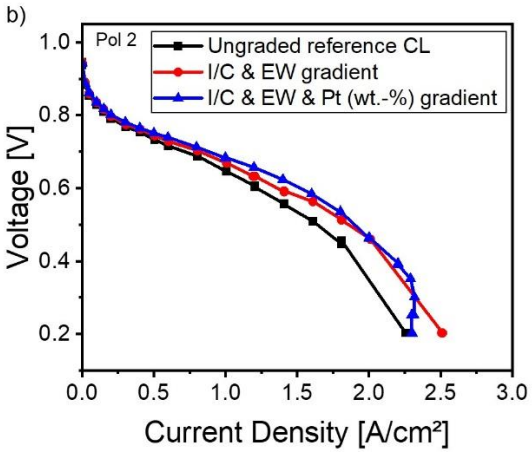

Figure S29 Polarization curves for the final optimized Gradient under Pol 2 conditions.

SI 4: Stability Test of the Gradient design under wet/dry Cycles

The samples were subjected to 100 wet/dry cycles, with humidity cycling between 0% and 100% relative humidity at 80°C, using an Air/N_2 gas flow at 50 L/h. Each cycle included a 3-minute hold at the respective humidity level before switching.

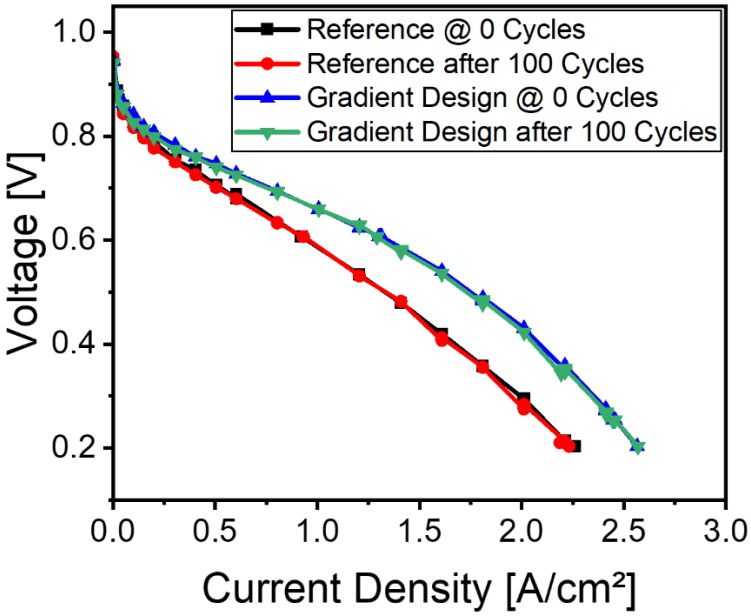

Figure S30 Stability Test of the reference and Gradient CL design after 100 wet/Dry cycles.

SI 5: Ungraded (Standard) vs. Gradient CL: Fabrication Process

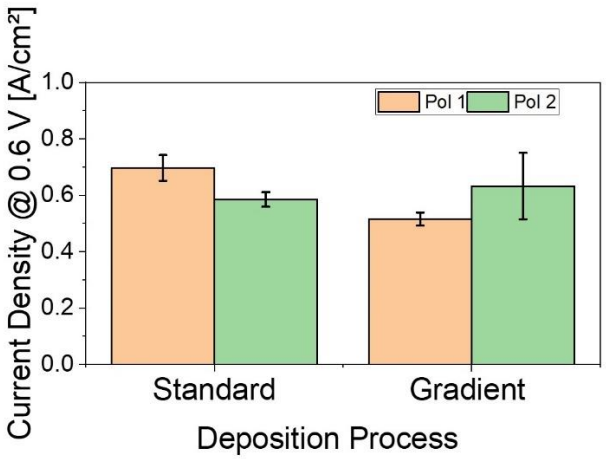

Figure S31 Comparison between the standard single layer deposition method and the gradient (three - layers) deposition method.

SI 6: Pre-optimization of CLs (ungraded Layers)

Here, we present the pre-optimization of CL compositions as a basis for developing graded cathodes. The aim was to systematically investigate how varying the I/C ratio affects the performance of ungraded CLs at different ionomer EW. Two commercially available Pt/C catalysts, Pt/XC72R and Pt/MSAC, were studied. For each selected EW (720, 830, and 980), the I/C ratio was varied stepwise from 0.7 to 0.9 to 1.1. This approach allowed for a detailed evaluation of the combined effects of ionomer content and chemical structure on PEMFC performance. As described in Methods, the CLs were tested under two different operating

conditions: Pol 1 (high stoichiometry, fully humidified) and Pol 2 (dry cathode conditions and lower stoichiometry). Figure S30 shows the current density at the cell voltage of 0.6 V assessed from the polarization curves.

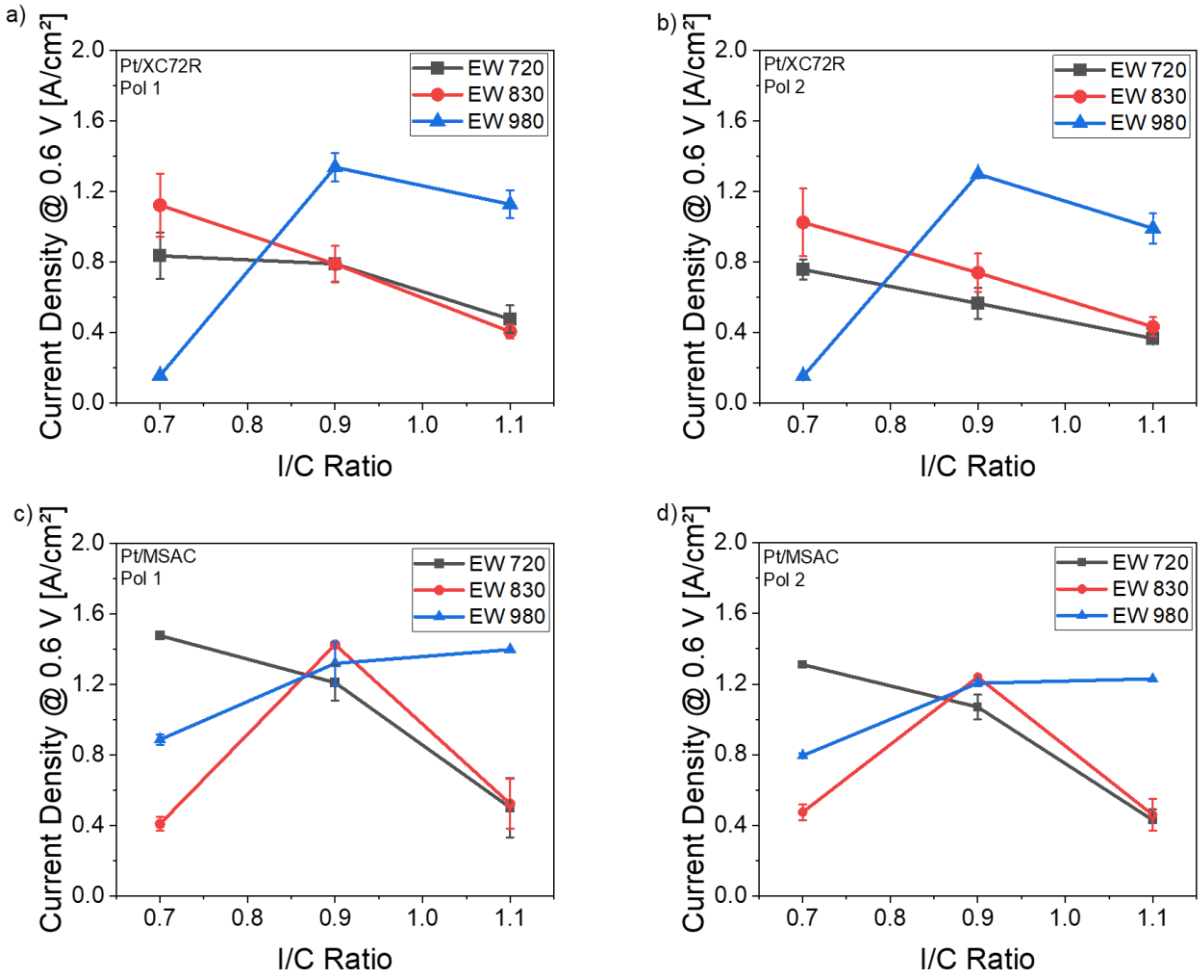

Figure S32 Current densities at 0.6 V: a) Influence of I/C ratio and EW variation at Pol 1 for Pt/XC72R, b) Influence of I/C ratio and EW variation at Pol 2 for Pt/XC72R, c) Influence of I/C ratio and EW variation at Pol 1 for Pt/MSAC, d) Influence of I/C ratio and EW variation at Pol 2 for Pt/MSAC.

Pt/XC72R Pol 1 and Pol 2

Figures S32a-b show the current density at 0.6 V as a function of I/C ratio and ionomer EW variation under Pol 1 (high humidity and high stoichiometry) and Pol 2 (dry cathode and low stoichiometry) respectively. The electrochemical performance of Pt/XC72R-based CLs, under both Pol 1 and Pol 2, show a strong dependence on both the EW and the I/C ratio, as reflected in the current density behavior. Although, the absolute current densities are slightly lower under Pol 2 conditions.

Under Pol 1 and for the CL with ionomer EW720, increasing the I/C ratio from 0.7 to 0.9 and then to 1.1 leads to a continuous decrease in the current density. A similar behavior is observed for the CL with ionomer EW830. In contrast, for EW980 an initial increase in the current density is observed when the I/C ratio first raises from 0.7 to 0.9, followed by a slight drop at an I/C ratio of 1.1. The initial increase in current density for EW980 as the I/C ratio is raised from 0.7 to 0.9 may be attributed to the fact that, at an I/C ratio of 0.7, both the lower intrinsic protonic conductivity and the reduced ionomer content do not provide sufficient proton conductivity within the CL [1–3].

In order to better understand these trends, EIS measurements at 1 A/cm² were performed, with results summarized in Table S1. Several aspects must be considered to interpret the influence of I/C ratio and EW variations under both Pol 1 and Pol 2 polarization conditions.

First, when varying the I/C ratio at a constant EW, it is observed that the ohmic resistance (R_{ohm}) remains generally unaffected. This suggests that R_{ohm} is primarily determined by the bulk properties of the membrane rather than by changes within the CL [4]. However, increasing the I/C ratio leads to a significant rise in both the cathode charge transfer resistance (R_c) and mass transport resistance (R_{diff}). This behavior may be attributed to the formation of thicker ionomer layers at higher I/C, which hinder oxygen access to the Pt nanoparticles, thereby slowing the ORR kinetics and increasing R_c. In addition, the reduced porosity due to thicker ionomer films leads to greater mass transport limitations, reflected in an increase in R_{diff} [1, 4, 5].

When varying the EW while keeping the I/C ratio constant, a different behavior is observed. R_{ohm} remains largely constant, reinforcing the interpretation that it is dominated by the membrane properties. However, increasing the EW from 720 to 980 results in a decrease in R_c and R_{diff}. This may be explained by the swelling characteristics of the ionomers: EW720 tends to swell more strongly than EW830 or EW980 [5]. As EW increases, swelling is reduced, leading to thinner ionomer films, better Pt accessibility for oxygen, increased porosity, and consequently lower R_c and R_{diff}. Therefore, using a higher EW ionomer under constant I/C ratios improve oxygen transport properties, and consequently PEMFC performance

Table S1 EIS results at 1 A/cm² for Pt/XC72R CLs at Pol 1 under various I/C and EW configurations.

mΩ.cm²	**Pt/XC72R (Pol 1)**								
	EW720			EW830			EW980		
	I/C 0.7	I/C 0.9	I/C 1.1	I/C 0.7	I/C 0.9	I/C 1.1	I/C 0.7	I/C 0.9	I/C 1.1
R_{ohm}	66.2 ± 0.76	67.1 ± 3.5		68.5 ± 5.2	94.7 ± 0.8			70.6 ± 4.6	66.4 ± 0.3
R_c	233.2 ± 28.6	373.8 ± 37.6		155.8 ± 18.2	315.7 ± 25.2			140 ± 0,025	184.4 ± 51.6
R_{diff}	18.3 ± 1.8	52 ± 1.7		11.4 ± 2.1	27.7 ± 0.4			20.3 ± 0,38	110.4 ± 56.7

Pt/MSAC Pol 1 and Pol 2

Figures S32c-d show the current density behavior at 0.6 V for the catalyst Pt/MSAC under Pol 1 conditions (high humidity and high stoichiometry) and Pol 2 conditions (dry cathode and low stoichiometry). The results reveal a strong dependence on both the ionomer EW and the I/C ratio. Analogous to the Pt/XC72R catalyst, the general trends under Pol 1 and Pol 2 are similar, although the absolute current density values under Pol 2 are slightly lower.

Notably, the overall behavioral pattern of the Pt/MSAC catalyst appears, at first glance, quite different from that of Pt/XC72R. This raises the question of the origin of these differences, especially given that both catalysts are commercially widespread and are often abbreviated as 40wt% Pt/C.

Under Pol 1 conditions, and for the CL containing the ionomer with EW720, a decrease in current density is observed as the I/C ratio increases from 0.7 to 0.9 to 1.1. For EW830 the current density first increases when the I/C ratio is raised from 0.7 to 0.9, followed by a decrease at I/C 1.1. At EW980, the current density continues to rise when increasing the I/C ratio from 0.7 to 0.9 to 1.1. However, the slope becomes noticeably shallower, indicating that a plateau is gradually being approached.

Before discussing the differences in behavior between the two catalysts, it is useful first to examine the EIS data at 1 A/cm² for the catalyst Pt/MSAC under Pol 1 and conditions, summarized in Table S2, following the same analytical approach used for the Pt/XC72R catalyst.

When keeping the EW constant but varying the I/C ratio, similar trends to those observed with Pt/XC72R are found. In other words, the EIS data support the current density behavior, showing that: R_{ohm} generally remains unaffected by the I/C variation, suggesting that it is primarily dependent on the bulk conductivity of the membrane [4].

For EW720, both R_c and R_{diff} increase as the I/C ratio is raised from 0.7 to 0.9 to 1.1. This is likely due to the thickening of the ionomer layers, which increasingly block oxygen access to Pt sites, an effect that is further exacerbated by ionomer swelling [1, 4, 5]. As a result, the microstructure and porosity of the CL become less favorable for mass transport and ORR.

For EW830, R_c and R_{diff} both decrease when increasing the I/C ratio from 0.7 to 0.9. The observed decrease in R_c for Pt/MSAC at EW830 as the I/C ratio increases may be attributed to improve the proton conductivity within the CL, enabling more efficient ORR kinetics [1–3]. Similarly, the decrease in R_{diff} suggests that the initially low ionomer content at I/C 0.7 is insufficient to support the proton, oxygen and water transport pathways within the CL. Increasing the I/C ratio to 0.9 improves the continuity of the ionomer network, leading to enhanced oxygen diffusion and enhanced water management, thereby reducing mass transport resistance. However, both R_c and R_{diff} increase at I/C 1.1, likely due to excessive thickening of the ionomer layer (amplified by ionomer swelling), which blocks Pt site oxygen accessibility and negatively affects the CL porosity [1, 4, 5].

At EW980, both R_c and R_{diff} consistently decrease when the I/C ratio is increased from 0.7 to 0.9 to 1.1. This behavior suggests that in this range, proton conductivity and the microstructural properties of the CL continue to improve, enhancing both ORR kinetics and mass transport (oxygen and water management).

Table S2 EIS data at 1 A/cm² for Pt/MSAC CLs at Pol 1 and Pol 2 for the respective I/C and EW variations.

mΩ.cm²	**Pt/MSAC (Pol 1)**								
	EW720			EW830			EW980		
	I/C 0.7	I/C 0.9	I/C 1.1	I/C 0.7	I/C 0.9	I/C 1.1	I/C 0.7	I/C 0.9	I/C 1.1
R_{ohm}	60.1	69.6 ± 2.1	74.3	71.3 ± 5.4	66.8	72.2	64.6 ± 2.2	59.3 ± 5.5	64.3
R_c	134.7	220.2 ± 29.2	870	526.5 ± 36	166.9	685.2	223 ± 11.4	179.3 ± 17.3	165.1
R_{diff}	2	17.2 ± 6.3	13	35 ± 3	20.7	314.4	37.6 ± 10.3	9.4 ± 3	20.7

Pt/XC72R vs. Pt/MSAC

A detailed comparison of the current density behavior between Pt/XC72R and Pt/MSAC reveals not only differences in the absolute performance levels but, more critically, systematic shifts in the current density patterns as a function of I/C ratio and ionomer EW. These shifts provide important insights into how the physicochemical properties of the catalyst materials influence the interaction with the ionomer phase and control CL performance.

For Pt/MSAC at EW980, the current density continues to increase up to an I/C ratio of 1.1, after which a plateau behavior suggests that further increases in I/C would likely lead to a performance decline. In contrast, for Pt/XC72R at EW980, the maximum current density is already reached at an I/C of 0.9, followed by a decrease. At EW830, Pt/MSAC exhibits a peak at I/C 0.9, whereas Pt/XC72R reaches its maximum earlier at I/C 0.7. For EW720, Pt/MSAC shows that at an I/C ratio of 0.7, the current density appears to reach a plateau, suggesting that further reductions in I/C may not lead to significant performance gains. This plateau-like behavior is similar to that observed for EW980, where the current density continued to increase from I/C 0.9 to 1.1 but with a diminishing slope, indicating a stabilization of performance. In contrast, for Pt/XC72R, based on the observed shift in the trends, it is expected that the current density would begin to decline already at lower I/C ratios than 0.7, although direct measurements for these conditions are not available.

This consistent leftward shift (toward lower I/C ratios) of the performance maximum in Pt/XC72R compared to Pt/MSAC can be directly attributed to their different physicochemical characteristics, previously reported in our study [6]:

- Electronic Conductivity: Pt/MSAC has a higher electronic conductivity than Pt/XC72R, enabling more efficient electron transport within the CL even at higher ionomer contents. In Pt/XC72R, the lower conductivity exacerbates transport limitations, leading to an earlier performance decline as the I/C ratio increases.
- Surface Chemistry: Pt/XC72R has a higher density of oxygen-containing surface groups (particularly carboxyl groups due to its surface treatment history [7]). These groups are prone to electrostatic repulsion with the sulfonate groups of the ionomer at low I/C ratios, leading to inhomogeneous ionomer coverage, especially in the vicinity of Pt particles [8]. This results in insufficient proton conduction pathways and partial catalyst site isolation, ultimately causing performance losses. In contrast, Pt/MSAC possesses a less oxygenated, more hydrophobic and graphitized surface, with a higher isoelectric point. This surface interacts with ionomer primarily via van der Waals and π-π interactions [8], which are less sensitive to ionomer content. Consequently, ionomer can still be adequately distributed even at relatively high or moderate I/C ratios without forming thick layers that block gas access. This results in better catalyst utilization and sustained proton transport, allowing Pt/MSAC to tolerate higher I/C ratios without a sharp performance drop.

Together, these factors explain why Pt/MSAC is able to tolerate higher I/C ratios before a performance decline sets in, while Pt/XC72R reaches its performance maximum and begins to deteriorate at lower ionomer contents.

SI 7: I/C & EW Gradient: PEM|1.1 EW720_0.9 EW830_0.7 EW980|GDL

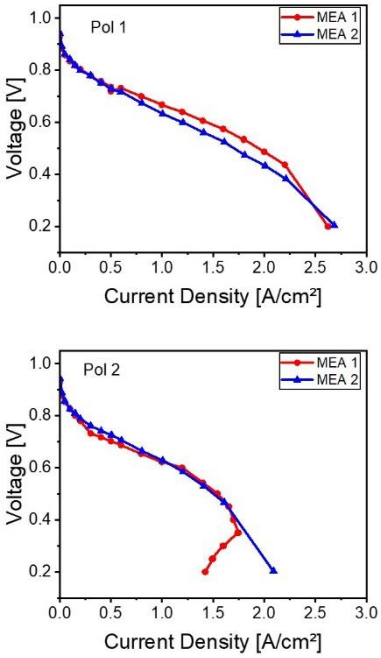

Figure S33 Polarization curves for the simultaneous I/C & EW gradient at Pol 1 and Pol 2.

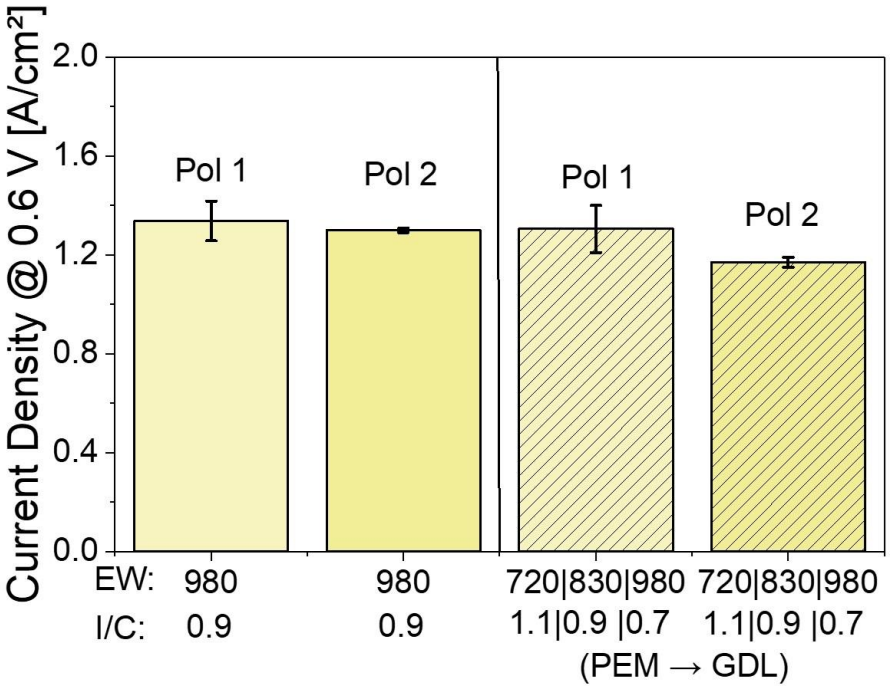

Figure S34 Current Densities at 0.6 V of the simultaneous I/C & EW gradient vs. Reference at Pol 1 and Pol 2.

SI 8: Calculations of Pt reduction costs and ionomer amount reduction

Pt reduction cost:

Table S3 Parameters for the cost calculation

Ungraded Reference CL				
Pol conditions	J [A/cm²]	U[V]	Pt loading [mg_{Pt}/cm^2]	Active surface Area [cm²]
Pol 1	1.33	0.6	0.18	25
Pol 2	1.29	0.6	0.18	25
Simultaneous I/C & EW & Pt/C loading gradient				
Pol Conditions	J [A/cm²]	U[V]	Pt loading [mg_{Pt}/cm^2]	Active surface Area [cm²]
Pol 1	1.73	0.6	0.18	25
Pol 2	1.52	0.6	0.18	25

$$P = U * I \qquad (1)$$

$$Platinum\ amount\ [mg] = Pt\ loading * active\ surface\ area \qquad (2)$$

$$Plainum\ amount \frac{mg}{W} = \frac{Platinum\ amount}{P} \qquad (3)$$

Platinum price [$/g_{Pt}]: 32 USD [9]

$$Costs\ \left[\frac{\$}{kW}\right] = Platinum\ price * Platinum\ amount \qquad (4)$$

Ionomer amount reduction:

Table S4 Parameters for the calculation of the ionomer amount reduction

Catalyst Layer	Pt loading [mg_{Pt}/cm^2]	I/C ratio
Ungraded reference layer	0.18	0.9
Near GDL (30 wt% Pt)	0.06	0.9
Middle (40 wt% Pt)	0.06	0.7
Near PEM (50 wt% Pt)	0.06	0.7

$$Amount\ of\ catalyst\ \left[\frac{mg}{cm^2}\right] = \frac{Pt\ loading\ [\frac{mg}{cm^2}]}{Pt\ loading\ wt\%} \quad (5)$$

$$Amount\ of\ carbon\ \left[\frac{mg}{cm^2}\right] = Amount\ of\ catalyst - Pt\ loading \quad (6)$$

$$Volume\ of\ carbon\ \left[\frac{cm^3}{cm^2}\right] = \frac{Amount\ of\ Carbon}{Density\ of\ Carbon} \quad (7)$$

Density of Carbon: 1.8 g/cm³

$$Volume\ of\ ionomer\ \left[\frac{cm^3}{cm^2}\right] = Volume\ Carbon * \frac{I}{C} ratio \quad (8)$$

$$Amount\ of\ ionomer\ \left[\frac{mg}{cm^2}\right] = Volume\ Ionomer * Density\ of\ ionomer \quad (9)$$

Density of Ionomer: 2.1 [g/cm³]

$$Ionomer\ savings\ \left[\frac{mg}{cm^2}\right] = Amount\ of\ ionomer\ (ungraded - Gradient) \quad (10)$$

SI 9: Application of CL Gradient on FUMAPEM-Membrane

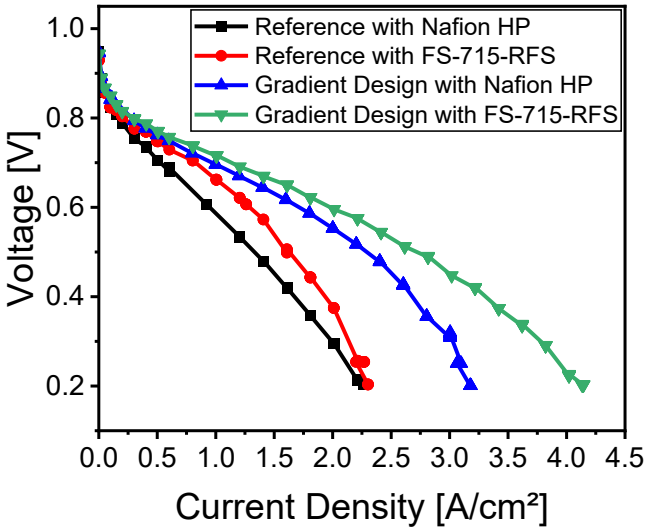

Figure S35 Comparison of Reference and Gradient CLs with Nafion HP and FumaPEM (FS-715-RFS).

SI 10: SEM-EDX of a reference CL

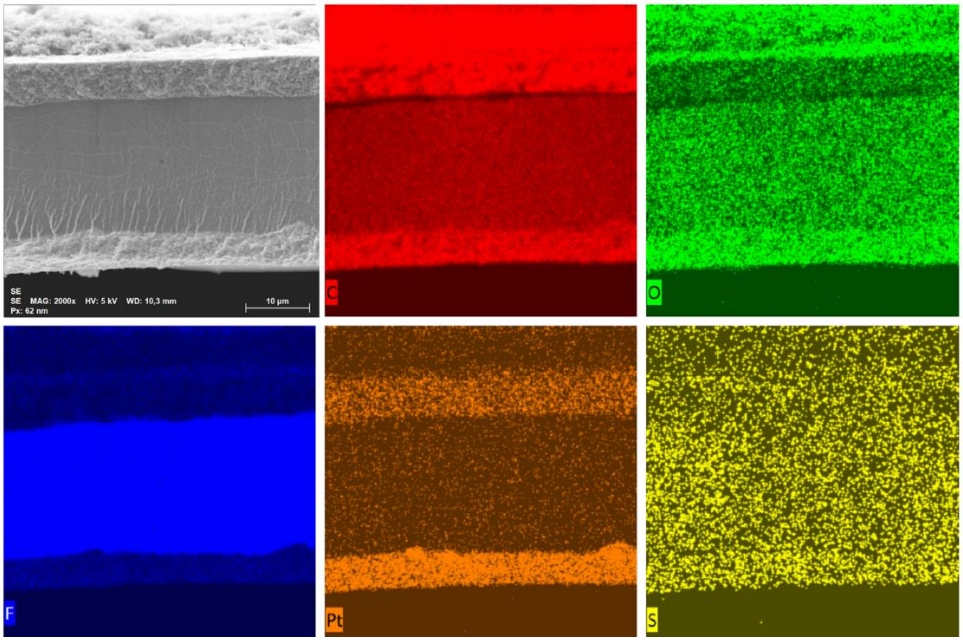

Figure S36 SEM-EDX of a reference CL.

Literature

[1] S. Shahgaldi, A. Ozden, X. Li und F. Hamdullahpur, "Cathode catalyst layer design with gradients of ionomer distribution for proton exchange membrane fuel cells", *Energy Conversion and Management*, Jg. 171, S. 1476–1486, 2018, doi: 10.1016/j.enconman.2018.06.078.

[2] K. KIM *et al.,* "Effect of Nafion® gradient in dual catalyst layer on proton exchange membrane fuel cell performance", *International Journal of Hydrogen Energy*, Jg. 33, Nr. 11, S. 2783–2789, 2008, doi: 10.1016/j.ijhydene.2008.03.015.

[3] Y.-G. Yoon, T.-H. Yang, G.-G. Park, W.-Y. Lee und C.-S. Kim, "A multi-layer structured cathode for the PEMFC", *Journal of Power Sources*, Jg. 118, 1-2, S. 189–192, 2003, doi: 10.1016/S0378-7753(03)00092-2.

[4] G.-Y. Chen *et al.,* "Gradient design of Pt/C ratio and Nafion content in cathode catalyst layer of PEMFCs", *International Journal of Hydrogen Energy*, Jg. 42, Nr. 50, S. 29960–29965, 2017, doi: 10.1016/j.ijhydene.2017.06.229.

[5] L. Xing, W. Shi, P. K. Das und K. Scott, "Inhomogeneous distribution of platinum and ionomer in the porous cathode to maximize the performance of a PEM fuel cell", *AIChE Journal*, Jg. 63, Nr. 11, S. 4895–4910, 2017, doi: 10.1002/aic.15826.

[6] Adib Caidi, Thomas Lange, Ivan Radev, Volker Peinecke, Fatih Özcan, Doris Segets, "Impact of Sonication Treatment on Physicochemical Properties of Carbon Blacks and Pt/C Catalysts in Proton Exchange Membrane Fuel Cells", *Particle & Particle Systems Characterization*, S. 1–23, 2025, doi: 10.1002/ppsc.202500057.

[7] J. E. Owejan, S. Bhargava und B. A. Litteer, "Surface Chemistry of Carbon Black Electrocatalyst Supports as a Result of a Commercial Synthethic Route", *ECS J. Solid State Sci. Technol.*, Jg. 1, Nr. 5, M33-M38, 2012, doi: 10.1149/2.004205jss.

[8] A. Szydło, "Preparation of Platinum-based Electrocatalytic Layers from Colloidal Dispersions with Adjusted Properties", 2020, doi: 10.17185/duepublico/73251.

[9] Online available at: https://www.goldpreis.de/platinpreis/.